IEEE Access
Multidisciplinary | Rapid Review | Open Access Journal

Received 26 June 2022, accepted 11 August 2022, date of publication 17 August 2022, date of current version 25 August 2022.

Digital Object Identifier 10.1109/ACCESS.2022.3199654

RESEARCH ARTICLE

A Vortex Electromagnetic Imaging Method Based on Two-Dimensional Matrix Compensation for Off-Grid Targets

CONG ZHANG[1], HANG YUAN[1], QUN ZHANG[1,2,3], AND YING LUO[1,2]

[1]Information and Navigation Institute, Air Force Engineering University, Xi'an 710077, China
[2]Collaborative Innovation Center of Information Sensing and Understanding, Xi'an 710077, China
[3]Key Laboratory for Information Science of Electromagnetic Waves, Ministry of Education, Fudan University, Shanghai 200433, China

Corresponding author: Qun Zhang (afeuzq@163.com)

This work was supported by the National Natural Science Foundation of China under Grant 61971434.

ABSTRACT Vortex electromagnetic (EM) wave has shown great potential in the field of radar imaging. Under the assumption that the target is located at the grid point, the compressed sensing (CS) algorithm is applied to vortex EM imaging and achieves high imaging quality. However, the off-grid target in the actual scene deviates from the grid points, resulting in the basis mismatch problem. This problem will lead to the mismatch between the assumed measurement matrix and the real echo signal and the degradation of the CS imaging performance. In order to solve this problem, a novel two-dimensional (2-D) joint off-grid imaging method is proposed by considering the gridding error as a multiplicative matrix and separating it via series expansion. This method compensates for errors in 2-D matrix directly instead of converting the 2-D matrix into the 1-D vector, which can not only solve the off-grid problem, but also reduce the storage of data acquisition and processing. Furthermore, the 2-D iterative adaptive algorithm (2DIAA) for the 2-D model is adopted to achieve better reconstruction performance and lower computational complexity. Finally, Simulation results show the effectiveness and robustness of the algorithm.

INDEX TERMS Vortex electromagnetic wave radar, compressive sensing, off-grid model, sparse signal reconstruction.

I. INTRODUCTION

The vortex electromagnetic (EM) wave is concerned increasingly in radar imaging [1], [2], [3], [4], [5], including generating vortex synthetic aperture radar simulation echo signal, analysing the angular Doppler shift and obtaining three-dimensional image of targets. The helical phase wavefront of vortex EM wave and the orthogonality of different orbital angular momentum (OAM) provide the potential of enhancing the imaging resolution [6]. More-detailed information of target can be obtained through emitting the vortex EM wave. Erenow, the investigation of vortex EM waves has been studied on radar imaging approaches [6] and OAM-generation methods with radiation pattern optimization [7]. In a radar imaging technique based on the OAM modulation of multiple-in--multiple-out (MIMO) mode is established by using a phased uniform circular array. The target detection capability can be enhanced by using the vortex EM wave radar. In [8], a system for generating high-order vortex beams is designed and the result indicated the vortex beams of high quality with several OAM modes can be generated. The generating and pattern optimization methods of OAM for vortex EM imaging was proposed in a few of articles [5], [9], [10], [11], and [12]. Due to the limitation of the topological charge of vortex electromagnetic waves, the improvement of azimuthal resolution in vortex imaging has become a key research area. Traditional methods such as Range-Doppler algorithm need to satisfy Nyquist's sampling law and the sparse reconstruction is able to break through the limitations of traditional methods for radar imaging and form high-resolution imaging [13].

The associate editor coordinating the review of this manuscript and approving it for publication was Hassan Tariq Chattha.

In sparse imaging, the perceptual matrix is usually determined by the imaging geometric relationships and the grid discretization strategy of the imaging region, thus requiring the assumption that all scattered points of the imaging scene are strictly distributed over the grid points, and such targets are called on-gird targets [14]. However, in the actual observation region, the scattering centers are continuously distributed, so the real scattering centers cannot fall exactly on the uniformly divided grid points, and the deviation from the grid will cause the basis mismatch problem, which affects the signal sparse reconstruction performance. Such targets are called off-grid targets. So, the mismatch correction method needs to be investigated. In addition, due to the limitation of restricted isometry property (RIP), it is not feasible to reduce the error by more dense grid division. There are currently two main solutions in the field of signal processing. The first approach is to perform signal processing in the continuous domain to avoid the off-grid problem, known as atomic norm minimization (ANM) [15], [16], [17], which is too complex for radar 2D imaging because it requires semidefinite programming. Another approach is to transform the problem into a parametric sparse representation problem by neglecting the higher-order terms through Taylor expansions and solving the grid deviation as a parameter, followed by a compensation process such as off-grid sparse Bayesian inference (OG-SBI) [14]. Our proposed method is based on the Taylor expansion and has the advantage of being less computationally intensive compared to the ANM method. The research of vortex EM wave imaging for off-grid targets is still in the initial stage. In [18], an off-grid variational sparse Bayesian inference (OG-VSBI) method is introduced to reconstruct the off-grid targets for vortex EM imaging. This method reconstructs the off-grid target based on SBL framework, achieves higher resolution and better imaging performance in noisy conditions. Nevertheless, the vectorization processing for the off-grid problem in range-azimuth plane, in which the columns of raw-data matrix are fit together end by end, not only leads to a high requirement of the computation and storage, but also causes the reconstruction performance degradation because of the separation from range and azimuth. To solve this problem, a 2-D joint imaging method for off-grid targets is proposed in this paper.

By analyzing the echo signal, an imaging model considering the gridding error is established based on the joint sparse imaging model. To reduce the load of storage and computation, we revise the joint sparse matrix by the one-order Taylor expansion. The 2-D cascade and vectoring processing are transformed to joint matrix processing. To improve the image performance, the adaptive dynamic grids instead of the refinement grids are applied to keep the restricted isometry property (RIP) and obtain high reconstruction probability. In addition, the 2DIAA [19] has been adopted to reconstruct the image for vortex EM wave radar. There is a high estimation accuracy for the results with satisfying speed. Finally, the effectiveness of the proposed method is verified by simulation.

The rest of this paper is organized as follows. Section II introduces off-grid sparse imaging model for vortex EM wave radar and presents the formulated optimization for it. Section III provides proposed algorithm. Section IV evaluates the effectiveness of the proposed methods by simulations. Finally, conclusions are drawn in Section V.

II. GUIDELINES FOR MANUSCRIPT PREPARATION

In conventional radar imaging process, the range resolution is determined with the bandwidth of the signal. The cross-range resolution is determined to the range of azimuth-angle during the imaging process and the wave length of the signal. For EM vortex imaging, the cross-range imaging can be obtained by utilizing the approximate dual relationship between the azimuthal angle and the OAM mode number [4]. In order to obtain high-order OAM, many methods [6], [7], [8] have been proposed. The uniform circular array (UCA) [20] is used to generate and receive the OAM beams in this paper.

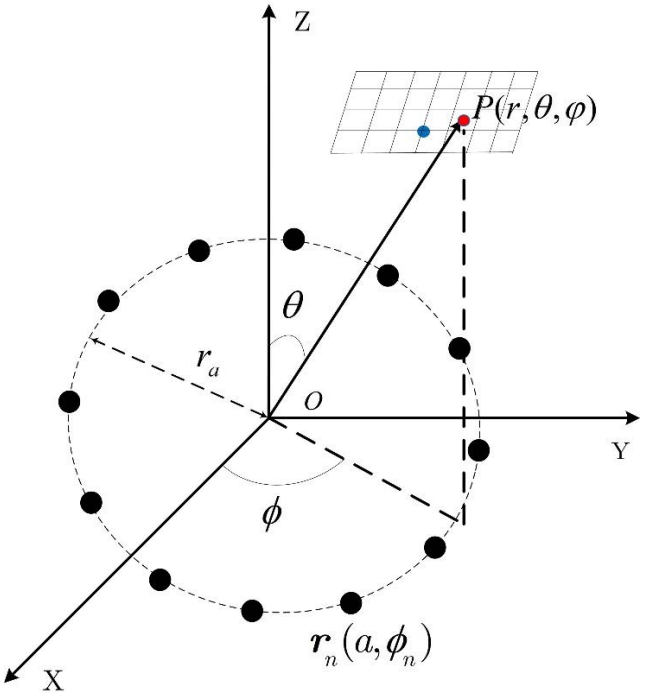

FIGURE 1. Radar observation coordinate for EM vortex imaging.

The radar observation model is shown in FIGURE 1. N antennas with equal spacing are located on a circle and the azimuthal position of each element is φ_n, the angle between radar line of sight and Z axis is θ, the P indicates the off-grid point scatter. The radius of circle is r_a. And the transmitted signal $s_n(t,\alpha)$ of the n^{th} antenna can be given by

$$s_n(t,\alpha) = \text{rect}(\frac{t}{T_p}) \cdot \exp(j2\pi(f_c t + \frac{1}{2}\mu t^2)) \cdot \exp(j\alpha\varphi_n) \quad (1)$$

where $\text{rect}(\frac{t}{T_p}) = \begin{cases} 1, -T_p/2 \le t \le T_p/2 \\ 0, \text{else} \end{cases}$, t denotes the fast time, μ is the chirp rate, T_p denotes the pulse width.

f_c is the carrier frequency of the signal, α is the OAM mode number and $\varphi_n = 2\pi(n-1)/N, n = 1, \ldots, N$. The total transmitted signal $s(t,\alpha)$ for an arbitrary scattering point $P(r,\theta,\varphi)$ in space can be expressed as

$$s(t,\alpha) = \sum_{n=1}^{N} \mathrm{rect}(\frac{t-t_n}{T_p}) \cdot \exp(j2\pi(f_c(t-t_n)+\frac{1}{2}\mu(t-t_n)^2)) \cdot \exp(j\alpha\varphi) \tag{2}$$

where $t_n = \hat{t} - \Delta r_{an}/c$, $\Delta r_{an} = r_a \sin\theta\cos(\varphi-\varphi_n)$, $\hat{t} = r/c$ and c is the light speed. When $\hat{t} \gg \Delta r_{an}/c$, $s(t,\alpha)$ can be rewritten as

$$\begin{aligned} & s(t,\alpha) \\ & \approx \sum_{n=1}^{N} \mathrm{rect}(\frac{t-\hat{t}}{T_p}) \cdot \exp\left\{j\pi\left[2f_c(t-\hat{t})+\mu(t-\hat{t})^2\right]\right\} \\ & \quad \cdot \exp\left\{j2\pi \cdot \frac{\Delta r_{an}}{c}\left[f_c+\mu(t-\hat{t})\right]\right\} \cdot \exp(j\alpha\varphi) \\ & = \mathrm{rect}(\frac{t-\hat{t}}{T_p}) \exp(\frac{j\alpha\pi}{2}) \cdot \exp(j\alpha\varphi) \cdot J_\alpha(2\pi f_c r_a \sin\theta/c) \\ & \quad \cdot \exp\left\{j\pi\left[2f_c(t-\hat{t})+\mu(t-\hat{t})^2\right]\right\} \end{aligned} \tag{3}$$

$J_\alpha(2\pi f_c r_a \sin\theta/c)$ is the first kind Bessel function of α^{th} order. Then the echo of $P(r,\theta,\varphi)$ can be expressed as

$$\begin{aligned} & s_r(t,\alpha) \\ & = \mathrm{rect}(\frac{t-\hat{t}}{T_p}) \cdot \sigma(r,\theta,\varphi)\exp(j\alpha\pi) \cdot \exp(j2\alpha\varphi) \\ & \quad \cdot \exp\left\{j\pi\left[2f_c(t-\hat{t})+\mu(t-\hat{t})^2\right]\right\} \cdot J_\alpha(2\pi f_c r_a \sin\theta/c) \end{aligned} \tag{4}$$

where $\sigma(r,\theta,\varphi)$ denotes the scattering coefficient for the point scatter $P(r,\theta,\varphi)$ which is unknown. All the antennas on the UCA are used to receive the echo scattered from the target, which is comprised of M scattering points. The signal received by the n^{th} antenna is multiplied by the term $e^{i\alpha\varphi_n}$. Accumulate the echoes of all array elements, and the array echo $s_r(t,\alpha)$ can be written as

$$\begin{aligned} & s_r(t,\alpha) \\ & = \exp(j\alpha\pi) \sum_{m=1}^{M} \mathrm{rect}(\frac{t-\hat{t}_m}{T_p})\sigma_m(r_m,\theta_m,\varphi_m) \cdot \exp(j2\alpha\varphi_m) \\ & \quad \cdot \exp\left\{j\pi\left[2f_c(t-\hat{t}_m)+\mu(t-\hat{t}_m)^2\right]\right\} J_\alpha^2(2\pi f_c r_a \sin\theta_m/c) \end{aligned} \tag{5}$$

where $\hat{t}_m = 2r_m/c$ and $\sigma_m(r_m,\theta_m,\varphi_m)$ indicates the radar cross section (RCS) of the m^{th} scattering point at spherical coordinate $P_m(r_m,\theta_m,\phi_m)$. When multiplying the reference signal

$$s_{ref}(t,\alpha) = \exp(j\alpha\pi)\mathrm{rect}(\frac{t}{T_p}) \cdot \exp\left\{j\pi\left[2f_c t+\mu(t)^2\right]\right\} \tag{6}$$

the echo $s_r(t,\alpha)$ at the basis frequency is

$$\begin{aligned} s_r(t,\alpha) = & \sum_{m=1}^{M} \cdot \exp\left[-j4\pi\mu t(r_m/c)\right] \cdot \exp\left[-j4\pi f_c(r_m/c)\right] \\ & \exp(j2\alpha\varphi_m)\sigma_m \mathrm{rect}(\frac{t-2r_m/c}{T}) \\ & \cdot J_\alpha^2(2\pi f_c r_a \sin\theta_m/c) \end{aligned} \tag{7}$$

the dechirped baseband echo signal can be written as

$$\begin{aligned} & s_r(t,\alpha) \\ & \approx \sum_{m=1}^{M} \cdot \int\int_{(r,\varphi)\in I} \sigma_{pq}(r,\varphi)\exp(j2\alpha\varphi_l) \\ & \quad \exp\left[-j4\pi\mu t(r/c)\right] \mathrm{d}r_m d\varphi_m J_\alpha^2(2\pi f_c r_a \sin\theta_m/c) \end{aligned} \tag{8}$$

$\sigma_{pq}(r,\varphi)$ denotes the reflection coefficient distribution function. When the target area is divided into $P \times Q$ grids and the reflection coefficient distribution function can be expressed as a matrix $\mathbf{\Omega} = [\sigma_{pq}]_{P\times Q} = [\sigma(r_P,\varphi_q)]_{P\times Q}$, where $(p = 1,2,\ldots,P, q = 1,2,\ldots,Q)$. The echo data can be discretized as $\boldsymbol{S} = [s_{lk}]_{L\times K}$, where L and K denote the range and azimuth sampling number, respectively. The discretized form of the signal model can be expressed as

$$\begin{aligned} \mathbf{S} = & \sum_{p=1}^{P}\sum_{q=1}^{Q} \sigma_{pq}\exp(j2l\varphi_q)J_l^2(2\pi f_c r_a \sin\theta_m/c) \\ & \exp\left[-j4\pi\mu k\Delta t(r_p/c)\right] \\ = & \mathbf{A}(\Phi)\,\mathbf{\Omega}\mathbf{B}(R) \end{aligned} \tag{9}$$

where Δt denotes the sampling interval of fast time, and

$$\begin{cases} \mathbf{A}(\Phi) = \begin{bmatrix} A_{11} & A_{12} & \cdots & A_{1Q} \\ A_{21} & A_{22} & \cdots & A_{2Q} \\ \vdots & \vdots & \ddots & \vdots \\ A_{L1} & A_{L2} & \cdots & A_{LQ} \end{bmatrix}, \\ \mathbf{B}(R) = \begin{bmatrix} B_{11} & B_{12} & \cdots & B_{1P} \\ B_{21} & B_{22} & \cdots & B_{2P} \\ \vdots & \vdots & \ddots & \vdots \\ B_{K1} & B_{K2} & \cdots & B_{KP} \end{bmatrix} \\ A_{lq} = \exp(j2l\varphi_q)J_l^2(2\pi f_c r_a \sin\theta_m/c) \\ B_{kp} = \exp\left[-j4\pi\mu k\Delta t(r_p/c)\right] \end{cases}$$

where X and Y denote the location of uniform grids in r- direction and $\varphi-$ direction, respectively. Correspondingly, the echo signal of off-grid target can be expressed as

$$\mathbf{S} = \mathbf{A}\left(\hat{\Phi}\right)\mathbf{\Omega}\mathbf{B}\left(\hat{R}\right) \tag{10}$$

where $\hat{R}$ and $\hat{\Phi}$ respectively denote the set of unbiased grid position in r- direction and φ-direction, respectively, and $\mathbf{\Omega}$ is the corrected reflection coefficient matrix.

Most of the current sparse recovery algorithms are based on that the scatter falling on the pre-divided grid points accurately, However, real targets are distributed in a continuous

scene and the moving state of non-cooperative target could not be described accurately like FIGURE 1, so the imaging performance is greatly reduced when this premise is not satisfied, which is mainly reflected in the imaging precision.

III. ELECTROMAGENETIC VORTEX IMAGING ALGORITHM BASED ON JOINT OG-IAA

A. CONVENTIONAL IMAGING FOR OFF-GRID TARGET

According to the sparse recovery framework, if the locations of the scatterers are regard as the parameters of the sparse dictionary $\boldsymbol{H}$, defining the vectorization operation as follows

$$vec(\mathbf{C}) = [c_1, \cdots, c_i, \cdots, c_I]^T, \quad i = n + (m-1)N \tag{11}$$

where $\mathbf{C} = [c_{mn}] \in \mathbb{C}^{M\times N}$. The parametric sparse representation model of (9) can be rewritten as

$$\hat{\boldsymbol{s}} = \boldsymbol{H}\left(\hat{R}, \hat{\Phi}\right)\boldsymbol{\alpha} + \boldsymbol{\varepsilon} \tag{12}$$

where $\begin{cases}\hat{R} = [\hat{r}_1, \hat{r}_2, \ldots, \hat{r}_{pq}, \ldots, \hat{r}_{PQ}] \\ \hat{\Phi} = [\hat{\varphi}_1, \hat{\varphi}_2, \ldots, \hat{\varphi}_{pq}, \ldots, \hat{\varphi}_{PQ}]\end{cases}$, $\boldsymbol{\alpha} = vec(\boldsymbol{\Omega})$, $\boldsymbol{\varepsilon}$ is the noise vector. $\hat{R}$ and $\hat{\Phi}$ are the location vector of the scatterer, respectively. To separate the assumed location and the gridding, the two-dimensional Taylor expression of $\boldsymbol{H}\left(\hat{R}, \hat{\Phi}\right)$ can be expressed as

$$\begin{aligned}&\boldsymbol{H}\left(\hat{R}, \hat{\Phi}\right) \\ &= \boldsymbol{H}(R, \Phi)\left(1 + (\hat{\Phi} - \Phi)\frac{\partial}{\partial \hat{\Phi}}\right. \\ &\left. + (\hat{R} - R)\frac{\partial}{\partial \hat{R}} + O\left(\left|(\hat{\Phi} - \Phi)\frac{\partial}{\partial \hat{\Phi}} + (\hat{R} - R)\frac{\partial}{\partial \hat{R}}\right|^2\right)\right)\end{aligned} \tag{13}$$

The model of (9) can be specifically expressed as

$$\begin{aligned}\hat{\boldsymbol{S}} = &\sum_{q=1}^{Q}\sum_{p=1}^{P}\sigma_{pq}\exp\left[j2l\varphi_q - j4\pi\mu k\Delta t(r_p/c)\right] \\ &J_l^2\left(2\pi f_c r_a \sin\theta_m/c\right) + O\left(|\delta|^2\right) \\ &+ \sum_{q=1}^{Q}\sum_{p=1}^{P}\sigma_{pq}\exp\left[j2l\varphi_q - j4\pi\mu k\Delta t(r_p/c)\right] \\ &(-j4\pi\mu k\Delta t(r_p/c)\delta r_{p,q}) \\ &+ \sum_{q=1}^{Q}\sum_{p=1}^{P}\sigma_{pq}\exp\left[j2l\varphi_q - j4\pi\mu k\Delta t(r_p/c)\right] \\ &(j2l\varphi_q\delta\varphi_{p,q})\end{aligned} \tag{14}$$

As can be seen from (9), the first term of (14) is same as the form of echo signal without gridding error. The second term is the echo signal with the gridding error on R- direction and can be rewritten as

$$\begin{aligned}&\boldsymbol{H}_1(R, \Phi)\boldsymbol{\alpha}_1 \\ &= \sum_{q=1}^{Q}\sum_{p=1}^{P}\sigma_{pq}\exp\left[j2l\varphi_q - j4\pi\mu k\Delta t(r_p/c)\right] \\ &(-j4\pi\mu k\Delta t(r_p/c)\delta r_{p,q})\end{aligned} \tag{15}$$

where

$$\begin{aligned}\boldsymbol{H}_1(R, \Phi) &= \left(\boldsymbol{h}_1^1, \boldsymbol{h}_2^1, \ldots, \boldsymbol{h}_{LK}^1\right)^T, \\ \boldsymbol{h}_i^1 &= \boldsymbol{h}_i \cdot -j4\pi\mu\Delta t(r_p/c)\left\lceil\frac{i}{K}\right\rceil\end{aligned}$$

where $\lceil\cdot\rceil$ is the ceiling function and $\odot$ denotes the Hadamard product. With the same procedure, the third term in (14), which contains the information of gridding error in $\boldsymbol{Y}$-direction, can be rewritten as

$$\begin{aligned}\boldsymbol{H}_2(R, \Phi)\boldsymbol{\alpha}_2 = (j2l\varphi_q\delta\varphi_{p,q})&\sum_{q=1}^{Q}\sum_{p=1}^{P}\sigma_{pq} \\ &\exp\left[j2l\varphi_q - j4\pi\mu k\Delta t(r_p/c)\right]\end{aligned} \tag{16}$$

where $\boldsymbol{H}_2(R, \Phi) = \left(\boldsymbol{h}_1^2, \boldsymbol{h}_2^2, \ldots, \boldsymbol{h}_{LK}^2\right)^T$, $\boldsymbol{h}_i^2 = \boldsymbol{h}_i \cdot j2\varphi_q\left\lceil\frac{i}{L}\right\rceil$.

Defining $\boldsymbol{\alpha}_1 = \boldsymbol{\alpha} \odot vec(\Delta\boldsymbol{R})$, $\Delta\boldsymbol{R} = [\delta r_{p,q}]_{PQ}$, $\boldsymbol{\alpha}_2 = \boldsymbol{\alpha} \odot vec(\Delta\Phi)$, $\Delta\Phi = [\delta\varphi_{p,q}]_{PQ}$, then the imaging model for off-grid targets can be expressed as

$$\begin{aligned}\hat{\boldsymbol{s}} &= \boldsymbol{H}(X, Y)\boldsymbol{\alpha} + \boldsymbol{H}_1(X, Y)\boldsymbol{\alpha}_1 + \boldsymbol{H}_2(X, Y)\boldsymbol{\alpha}_2 + \boldsymbol{\varepsilon}_0 \\ &= [\boldsymbol{H}(X, Y), \boldsymbol{H}_1(X, Y), \boldsymbol{H}_2(X, Y)]\begin{bmatrix}\boldsymbol{\alpha} \\ \boldsymbol{\alpha}_1 \\ \boldsymbol{\alpha}_2\end{bmatrix} + \boldsymbol{\varepsilon}_0 \\ &= \boldsymbol{H}_0\boldsymbol{\alpha}_0 + \boldsymbol{\varepsilon}_0\end{aligned} \tag{17}$$

where $\boldsymbol{H}_0 \in \mathbb{C}^{LK\times 3PQ}$ is the partitioned matrix, $\boldsymbol{\alpha}_0 \in \mathbb{C}^{3PQ}$ contains the information of reflection coefficient and gridding error in R $-$ Φ plane, $\boldsymbol{\varepsilon}_0 = \boldsymbol{\varepsilon} + \boldsymbol{H}\boldsymbol{\alpha} \odot O(\delta^2)$ denotes the noise and the high order component of the off-grid error. Then the imaging problem can be transformed to the optimization problem as follows

$$\hat{\boldsymbol{\alpha}}_0 = \arg\min_{\boldsymbol{\alpha}_0}\left\{\left\|\hat{\boldsymbol{s}} - \boldsymbol{H}_0\boldsymbol{\alpha}_0\right\|_2^2 + \rho\left\|\boldsymbol{\alpha}_0\right\|_P\right\}, \quad 0 \le P \le 1 \tag{18}$$

By obtaining the reflection coefficients of the off-grid scatterer by $\boldsymbol{\alpha}$ and correcting the positions of the off-grid scatterer by $\boldsymbol{\alpha}_1$ and $\boldsymbol{\alpha}_2$, the high-resolution imaging for off-grid target can be achieved. Obviously, the optimization problem can be solved by other similar methods, such as the off-grid sparse Bayesian inference (OG-SBI) algorithm. However, the size of computation for (18) is about $O(LK \times 3PQ)$, which is larger than the resolution requirement.

B. OFF-GRID TARGETS IMAGING ALGORITHM BASED ON JOINT 2D-MODEL

Approximating the $A(\hat{\Phi})$ and $B(\hat{R})$ by the first-order Tylor expansion around the predefined grids r and φ respectively, it yields

$$\hat{S} = \left[\mathbf{A}(\Phi) + \frac{\partial \mathbf{A}(\Phi)}{\partial \Phi}\mathbf{\Delta}\Phi\right]\mathbf{\Omega}\left[\mathbf{B}(R) + \frac{\partial \mathbf{B}(R)}{\partial R}\mathbf{\Delta}R\right] \quad (19)$$

where $\frac{\partial \mathbf{A}(\Phi)}{\partial \Phi} = [\frac{\partial \mathbf{A}(\Phi_{11})}{\partial \varphi_1}, \cdots, \frac{\partial \mathbf{A}(X_{LQ})}{\partial \varphi_q}]$, $\frac{\partial B(R)}{\partial R} = [\frac{\partial B(R_{11})}{\partial r_1}, \cdots, \frac{\partial B(R_{KP})}{\partial r_p}]$, $\Delta X = diag(\hat{\Phi} - \Phi)$, $\Delta Y = diag(\hat{R} - R)$. We can get the following joint matrix model $\hat{S}$

$$\begin{aligned}
&\left[\mathbf{A}(\Phi)\frac{\partial \mathbf{A}(\Phi)}{\partial \Phi}\right]\begin{bmatrix}\mathbf{I}\\ \mathbf{\Delta X}\end{bmatrix}\mathbf{\Omega}\begin{bmatrix}\mathbf{I}\\ \mathbf{\Delta Y^T}\end{bmatrix}\left[\mathbf{B}(R)\frac{\partial \mathbf{B}(R)}{\partial R}\right]^T\\
&= \left[\mathbf{A}(\Phi)\frac{\partial \mathbf{A}(\Phi)}{\partial \Phi}\right]\begin{bmatrix}\mathbf{\Omega} & \mathbf{U_2}\\ \mathbf{U_1} & \mathbf{U_3}\end{bmatrix}\left[\mathbf{B}(R)\frac{\partial \mathbf{B}(R)}{\partial R}\right]^T\\
&= \mathbf{\Psi}_\varphi \tilde{\mathbf{\Omega}} \Psi_r\\
&= \hat{\boldsymbol{S}}
\end{aligned} \quad (20)$$

where

$$\begin{aligned}
\mathbf{\Psi}_\varphi &= \left[\boldsymbol{A}(\Phi)\frac{\boldsymbol{A}}{\partial \Phi}\right] \in \mathbb{C}^{L\times 2\,Q}\\
\mathbf{\Psi}_r &= \left[\boldsymbol{B}(R)\frac{\boldsymbol{B}}{\partial R}\right]^T \in \mathbb{C}^{2P\times K}\\
\tilde{\mathbf{\Omega}} &= \begin{bmatrix}\mathbf{\Omega} & \mathbf{\Omega}\odot\Delta\mathbf{R}\\ \mathbf{\Omega}\odot\Delta\mathbf{\Phi}^T & \boldsymbol{U}_2\end{bmatrix} \in \mathbb{C}^{2Q\times 2\,P}
\end{aligned} \quad (21)$$

where $\mathbf{\Psi}_\varphi$ and $\mathbf{\Psi}_r$ denote the corrected sparse basis matrices in the azimuth and range direction, respectively. The structure of (20) is coincidence with the two-dimensional CS expression, which we convert the 1-D vector form in (17) into 2-D matrix form. If we can get $\tilde{\mathbf{\Omega}}$ from (20), the off-grid error in EM vortex imaging can be corrected by the matrix $\mathbf{\Omega}$, $\Delta\mathbf{R}$ and $\Delta\mathbf{\Phi}$. Then, the sparse sampling signal $\hat{\boldsymbol{S}}$ can be expressed as

$$\hat{\boldsymbol{S}} = \mathbf{\Psi}_\varphi \tilde{\mathbf{\Omega}} \tilde{\Psi}_r \quad (22)$$

Since $L < Q$ and $K < P$, the sparse recovery problem in (22) is underdetermined. Considering the presence of noise, the sparse matrix $\tilde{\mathbf{\Omega}}$ can be recovered by minimizing the l_0-norm of $\tilde{\mathbf{\Omega}}$.

$$\min_{\tilde{\mathbf{\Omega}}} \left\|\tilde{\mathbf{\Omega}}\right\|_0 \quad \text{s.t.} \left\|\hat{\boldsymbol{S}} - \tilde{\mathbf{\Phi}}_\varphi \tilde{\mathbf{\Omega}} \tilde{\Phi}_r\right\|_2^2 < \varepsilon \quad (23)$$

where $\|\cdot\|_2$ denotes the 2-parametric form of the matrix, and ε is related to the noise variance. Moreover, the novel sparse reconstruction model for off-grid targets, which should be proposed to directly work on the 2-D sparse matrix. The two-dimensional iterative adaptive approach (2DIAA) which directly solves 2D sparse signal models is chosen to enhance the computational efficiency. Here is the brief introduction of the 2DIAA and more details are shown in [16]. IAA is a nonparametric estimation method based on weighted least squares, the 2-D IAA is carried to solve 2-D sparse signals.

TABLE 1. Algorithm: OGIAA for vortex radar imaging.

Input: echo signal $\hat{\boldsymbol{S}}_0$; measurement matrices $\mathbf{\Psi}_\varphi$ and $\mathbf{\Psi}_r$.

Output: corrected reflection coefficient matrix $\mathbf{\Omega}$, gridding errors in r- direction $\Delta\boldsymbol{R}$ and gridding errors in φ- direction $\Delta\mathbf{\Phi}$

Step 1: Pulse Compression

1) Dechirping: $\mathbf{S}_r = \mathbf{S} \bullet \mathbf{S}_{ref}^*$;

2) Divide imaging area into grids;

Step 2: 2-D off-grid compensation via 2-D IAA

Initialization:

$\mathbf{U}_0 = 0, \beta_0 = 0, \mathbf{R}_0 = \mathbf{S}_r, \mathbf{P}_0 = 0, \rho_0 = \|\mathbf{R}_0\|_F^2, \mathbf{r} = vec(\mathbf{R})$

For $t = 1,2,...,T; j = 1,2,...,J;$

$\mathbf{P}_{j+1} = \mathbf{R}_j + \beta_j \mathbf{P}_j$

$\mathbf{W}_j = \mathbf{\Psi}_\varphi(\mathbf{\Sigma} \odot (\mathbf{\Psi}_\varphi{}^H \mathbf{P}_{j+1} \mathbf{\Psi}_r{}^H))\mathbf{\Psi}_r$ where the components of $\mathbf{\Sigma}$ are given by

$\mathbf{\Sigma}_{ij} = \left|\tilde{\mathbf{\Omega}}_{ij}\right|^2, i = 1,...,2P, j = 1,...,2Q$

$\alpha_j = \rho_j / (1_Q^T(\mathbf{P}_{j+1}^* \odot \mathbf{W}_j)1_P)$

$\mathbf{U}_{j+1} = \mathbf{U}_j + \alpha_l \mathbf{P}_{j+1}$

$\mathbf{R}_{j+1} = \mathbf{R}_{j+1} - \alpha_j \mathbf{W}_j$

$\rho_{j+1} = \|\mathbf{r}_{j+1}\|_F^2$

$\rho_{j+1} = \rho_{j+1} / \rho_j$

Stop until after several iterations or until $\sqrt{\rho_{j+1}} < \varepsilon \|\hat{\mathbf{S}}_r\|_F$

Result $\mathbf{U} = \mathbf{U}_{j+1}$

$\tilde{\mathbf{\Omega}}^{(t+1)} = \mathbf{\Sigma}^{(t)} \odot (\mathbf{\Psi}_\varphi^H \mathbf{U} \mathbf{\Psi}_r^H)$

End

Now we got the off-grid 2D-IAA(OG-IAA) for EM vortex imaging which is shown in TABLE 1.

Through the above analysis, the entire algorithm flow chart is shown in FIGURE 2.

C. COMPLEXITY ANALYSIS AND SNR

This section begins with a brief analysis of the computational complexity of the algorithm. Vectorization processing method in (17) and the sparse reconstruction problem scale based on joint 2D IAA proposed are analyzed separately as follows. It is clear that the size of (22) including $\boldsymbol{H}_0 \in \mathbb{C}^{KL\times 3PQ}$ and $\boldsymbol{\alpha}_0 \in \mathbb{C}^{3PQ}$ with $3(KL+1)PQ$ elements is much larger than the size of (39) including $\mathbf{\Psi}_\varphi \in \mathbb{C}^{L\times 2Q}$,

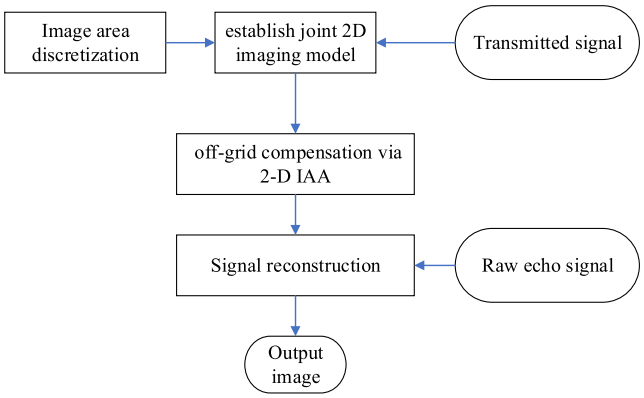

FIGURE 2. Flowchart of the OG-2DIAA-based EM vortex imaging.

$\mathbf{\Psi}_r \in \mathbb{C}^{2P\times K}$ and $\tilde{\mathbf{\Omega}} \in \mathbb{C}^{2P\times 2Q}$ with $2LQ + 2PK + 4PQ$ elements. Therefore, the 2-D matrix signal model can save a lot of computing memory, compared with the conventional 1-D vector signal model.

IV. EXPERIMENTS

To validate the method proposed, a series of simulate experiments are carried out to demonstrate the effectiveness of the proposed algorithms. The key parameters of the experimental setup are listed in TABLE 2.

A. 2D IMAGING PERFORMANCE

In the process of sparse reconstruction as we mentioned earlier, the imaging area needs to be divided into discrete grids. Theoretically, the finer the grid size is divided, the higher the imaging resolution that may be obtained. But the grid cannot be set to infinity due to the limitation of calculation volume. We design that the imaging area is 20m $\times$ 80° which is divided into 41 $\times$ 41 imaging cells. In the first experiment, 4 scatter points on grid is set as targets in imaging area to compare the performance of different methods. The point target embraces 4 scatterers which are located on (700m, 54°, 30°), (700m, 54°, 60°), (705m, 54°, 30°), (705m, 54°, 60°) respectively. Here we show the results of target reconstruction based on OG-2DIAA method target under ideal conditions and compare them with fast Fourier transform (FFT) method, orthogonal matching pursuit (OMP), and off-grid variational sparse Bayesian inference (OGVSBI) method [14] in FIGURE 3. From FIGURE 3.(b), The FFT method is to directly do FFT transform in the distance direction and azimuth direction of the radar imaging respectively to get the image, OMP is a greedy algorithm for signal recovery from random measurements. we can see the FFT imaging method does not successfully reconstruct the correct position of the target points. According to FIGURE 3.(c)-(e), the imaging results of OMP, OGSBI and OG-2DIAA successfully demonstrate location of the target points. It is obviously that the OG-2DIAA has a higher resolution than FFT method, and it is slightly better than OMP.

Next, we test the effectiveness of method proposed in a noisy environment. The noise is white Gaussian noise and the SNR is 13dB.

TABLE 2. Paramengts in the simulations.

Paraments	value
Topological charge α	[-10,10]
Number of scattering points N	4
Carrier Frequency f_c	10GHz
Array radius a	0.10m
Signal Bandwidth B	500MHz

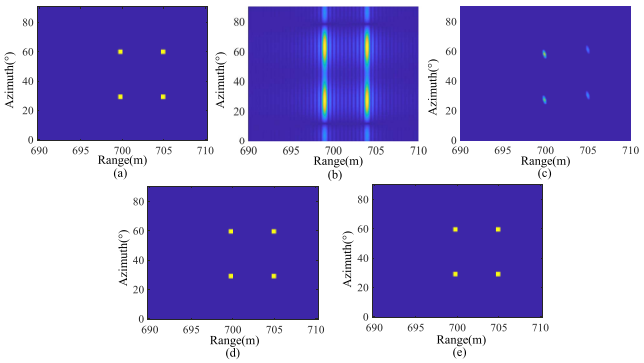

FIGURE 3. Imaging results under ideal circumstances. (a) real ground location. (b) FFT. (c) OMP. (d) OG-VSBI. (e) OG-2DIAA.

Gaussian noise was added to each pulse to simulate the noise environment. The imaging results under different noise conditions are shown in FIGURE 4, It can be seen that the robustness of the proposed method in the presence of noise is significantly stronger than FFT method and OMP. Both OG-VSBI method and OG-2DIAA can accurately reconstruct targets in the presence of noise.

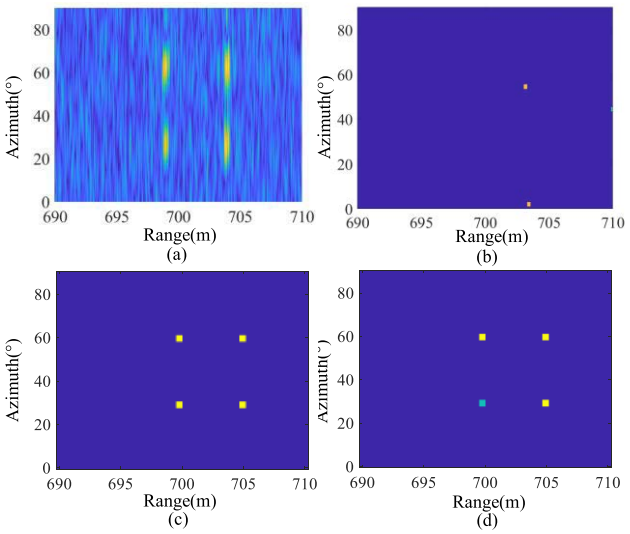

FIGURE 4. Imaging results with SNR = 13dB. (a) FFT. (b) OMP (C) OG-VSBI (d) OG-2DIAA.

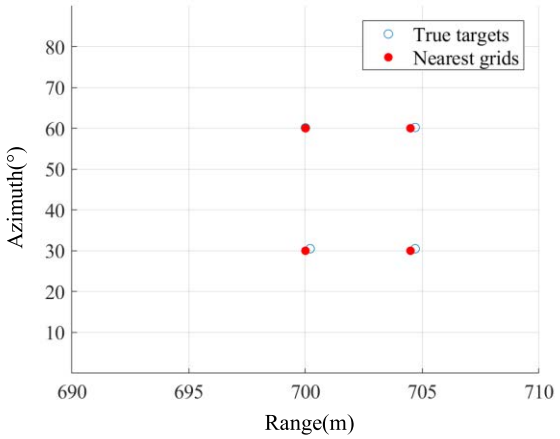

FIGURE 5. Off-grid targets in real ground location.

B. EXPERIMENT FOR OFF-GRID TARGETS

In practical environments, there are more than one off-grid target in imaging area. In the first experiment, we assume that there are 4 off-grid points targets to compare the reconstruction performance of different methods. The locations of 4 targets are shown in FIGURE 5. As is seen form FIGURE 5, the range direction and azimuth direction of reconstruction results are shown when SNR is 25dB and 5dB, respectively. As is shown in FIGURE 6(a) and (b), when SNR is 25 dB, the proposed method and OGVSBI can reconstruct 4 points targets accurately, while OMP and 2DIAA still suffers from off-grid targets and cannot reconstruct all point targets. When SNR is 5dB as shown in FIGURE 6(c) and (d), side lobe jamming occurs in all methods and resulting in inaccurate reconstruction. But it is apparently that the imaging results of OMP and 2DIAA are worse than OGVSBI method and proposed method due to the influence of off-grid targets. Moreover, the mean square error (MSE) of the target location estimation through 200 Monte Carlo trials is shown in FIGURE 6 to do de-quantitative comparison of performance at different SNRs. it can be seen that the MSE of all the methods is relatively high in the low SNR condition. With increasing SNR, all methods' error decrease, while the OGSBI method and the proposed method have a better performance than OMP and 2DIAA, which still suffers from off-grid effect. Moreover, when SNR is 10dB, the reconstruction performance of proposed method is better than OGVSBI. In addition, the reconstruction performance of all methods in different off-grid conditions is also analyzed. In FIGURE 7(a) and(b), 10% and 50% random deviation are added in both range direction and azimuth direction of point targets, respectively. It is seen that the higher the ratio of off-grid targets, the worse the reconstruction performance. In general, the proposed method is significantly better than OMP and 2DIAA, and slightly better than OGVSBI when the SNR is low, both in the high or low ratio of off-grid targets conditions.

To compare the computational complexity of the methods, we review the range sampling number K and the azimuth sampling number L, the number of grids of imaging area is P and Q in range-direction and azimuth-direction respectively.

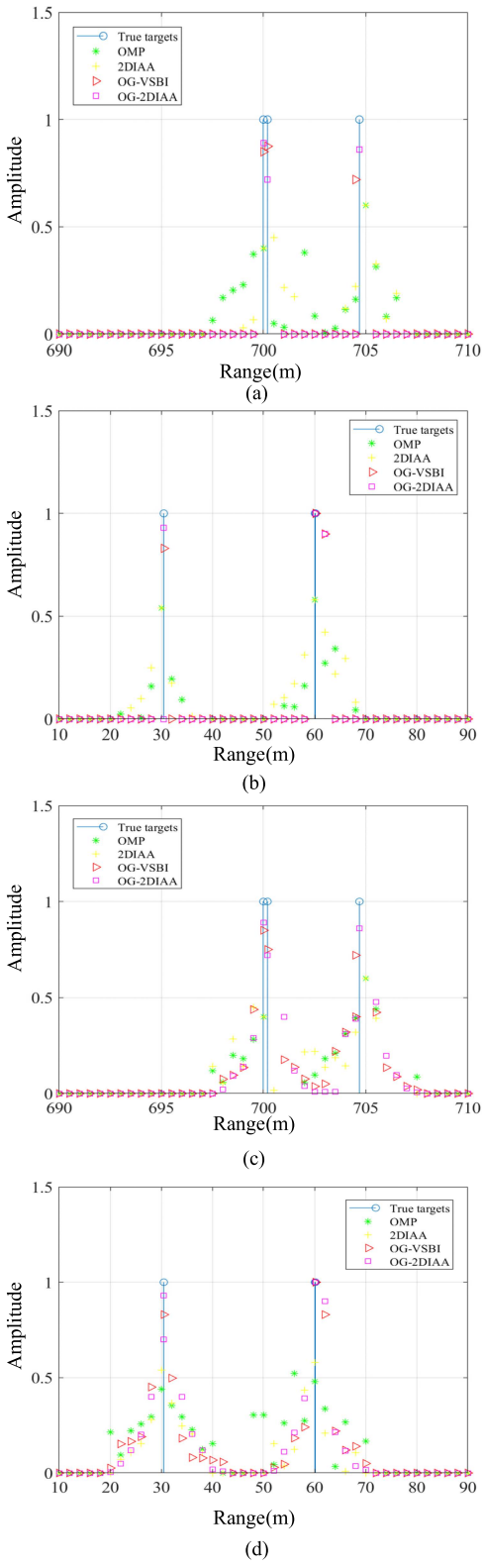

FIGURE 6. Range direction and azimuth direction of reconstruction result when SNR is 25dB and 5dB, respectively. (a) Range direction with SNR is 25dB. (b) Azimuth direction with SNR is 25dB. (c) Range direction with SNR is 5dB. (d) Azimuth direction with SNR is 5dB.

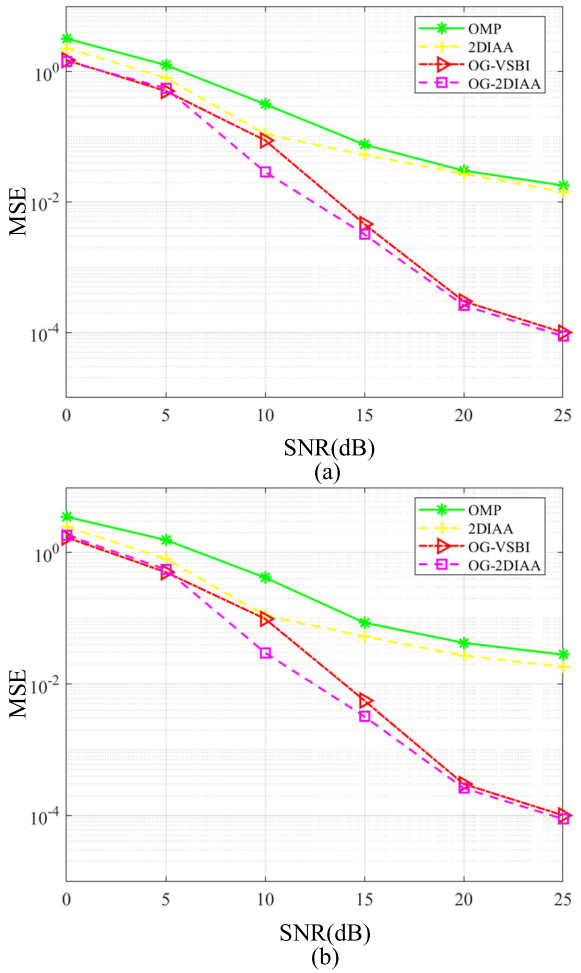

FIGURE 7. Reconstruction performance for 10% off-grid scatters and 40% off-grid scatters by MSE versus SNR. (a) 10% off-grid error of scatters. (b) 40% off-grid error of scatters.

And the point number of target is M. The computational size of OMP is about $O(KL \times PQ \times M)$, while the computational size of OGVSBI is about $O((KL)^2 \times 3PQ)$ in one iteration. For 2DIAA and OG-2DIAA, the computational size is about $O((K + L) \times PQ)$ and $O((K + L) \times 3PQ)$ in one iteration, respectively. In above simulation experiments, the running time of the algorithm imaging for OMP, 2DIAA, OG-VSBI and OG-2DIAA is about 32.2452s, 18.1425s,210.2693s and 35.2357s, respectively.

V. CONCLUSION

In this paper, a novel imaging method for off-grid targets in vortex EM wave is proposed. Through the direct 2D matrix error correction instead of vectorization of matrices, we establish a two-dimensional sparse matrix reconstruction model for off-grid targets. Compared with the available imaging methods, our approach is proven to be more effective and accurate with less amount of computation through numerical simulations. Furthermore, the proposed method has a better performance in lower SNR and worse off-grid ratio.

REFERENCES

[1] Y. Luo, Y.-J. Chen, Y.-Z. Zhu, W.-Y. Li, and Q. Zhang, "Doppler effect and micro-Doppler effect of vortex-electromagnetic-wave-based radar," *IET Radar Sonar Navigat.*, vol. 14, no. 25, pp. 2–9, Jan. 2019, doi: 10.1049/IET-RSN.2019.0124.

[2] Y. Luo, Y. Chen, Y. Zhu, W. Li, and Q. Zhang, "Doppler effect and micro-Doppler effect of vortex-electromagnetic-wave-based radar," *IET Radar, Sonar Navigat.*, vol. 14, no. 1, pp. 2–9, Jan. 2020, doi: 10.1049/IET-RSN.2019.0124.

[3] P. Wang, Y. Fang, J. Chen, W. Yang, and Z. Men, "Electromagnetic vortex synthetic aperture radar signal simulating method, involves calculating target scattering coefficient value according to simulation parameters, and generating vortex synthetic aperture radar simulation echo signal," CN Patent 107 656 253-A.

[4] H. Ma, K. Lv, and H. Liu, "Electromagnetic vortex wave based synthetic aperture radar three-dimensional imaging method, involves obtaining focused image of echo signal, and compressing focused image of echo signal to obtain three-dimensional image of target," CN Patent 110 412 571-A.

[5] X. Bu, Z. Zhang, L. Chen, X. Liang, H. Tang, and X. Wang, "Implementation of vortex electromagnetic waves high-resolution synthetic aperture radar imaging," *IEEE Antennas Wireless Propag. Lett.*, vol. 17, no. 5, pp. 764–767, May 2018, doi: 10.1109/LAWP.2018.2814980.

[6] C. Deng, W. Chen, Z. Zhang, Y. Li, and Z. Feng, "Generation of OAM radio waves using circular vivaldi antenna array," *Int. J. Antennas Propag.*, vol. 2013, pp. 1–7, Apr. 2013, doi: 10.1155/2013/847859.

[7] K. Liu, Y. Cheng, Z. Yang, H. Wang, Y. Qin, and X. Li, "Orbital-angular-momentum-based electromagnetic vortex imaging," *IEEE Antennas Wireless Propag. Lett.*, vol. 14, pp. 711–714, 2015, doi: 10.1109/LAWP.2014.2376970.

[8] K. Liu, H. Liu, Y. Qin, Y. Cheng, S. Wang, X. Li, and H. Wang, "Generation of OAM beams using phased array in the microwave band," *IEEE Trans. Antennas Propag.*, vol. 64, no. 9, pp. 3850–3857, Sep. 2016, doi: 10.1109/TAP.2016.2589960.

[9] L. Li, Y. Zheng, Q. Feng, H. Xue, R. Xi, and Q. Shao, "Method for generating low sidelobe vortex beam based on multi-ring array for use in wireless communication and radar imaging applications, involves determining power of scan parameter, and determining lowest sidelobe power of scan parameter," CN Patent 110 444 903-A.

[10] W. Lin, T. Lujing, L. Zhongyu, W. Junjie, and Y. Jianyu, "A new air target orientation observations based on electromagnetic vortex radar," in *Proc. 6th Asia–Pacific Conf. Synthetic Aperture Radar*, Nov. 2019, p. 4.

[11] K. Liu, Y. Cheng, X. Li, H. Wang, Y. Qin, and Y. Jiang, "Study on the theory and method of vortex-electromagnetic-wave-based radar imaging," *IET Microw., Antennas Propag.*, vol. 10, no. 9, pp. 961–968, Jun. 2016, doi: 10.1049/IET-MAP.2015.0842.

[12] K. Liu, Y. Cheng, Y. Gao, X. Li, Y. Qin, and H. Wang, "Super-resolution radar imaging based on experimental OAM beams," *Appl. Phys. Lett.*, vol. 110, no. 16, Apr. 2017, Art. no. 164102, doi: 10.1063/1.4981253.

[13] S. R. DeGraaf, "SAR imaging via modern 2-D spectral estimation methods," *IEEE Trans. Image Process.*, vol. 7, no. 5, pp. 729–761, May 1998, doi: 10.1109/83.668029.

[14] Z. Yang, L. Xie, and C. Zhang, "Off-grid direction of arrival estimation using sparse Bayesian inference," *IEEE Trans. Signal Process.*, vol. 61, no. 1, pp. 38–43, Jan. 2013, doi: 10.1109/TSP.2012.2222378.

[15] G. Tang, B. N. Bhaskar, P. Shah, and B. Recht, "Compressed sensing off the grid," *IEEE Trans. Inf. Theory*, vol. 59, no. 11, pp. 7465–7490, Nov. 2013, doi: 10.1109/TIT.2013.2277451.

[16] C. Zhou, Y. Gu, X. Fan, Z. Shi, G. Mao, and Y. D. Zhang, "Direction-of-arrival estimation for coprime array via virtual array interpolation," *IEEE Trans. Signal Process.*, vol. 66, no. 22, pp. 5956–5971, Nov. 2018, doi: 10.1109/TSP.2018.2872012.

[17] H. Jiang, W. G. Tang, and S. X. Pang, "Off-grid DOA estimation for nested array using atomic norm minimisation," *Electron. Lett.*, vol. 54, no. 23, pp. 1344–1345, Nov. 2018, doi: 10.1049/EL.2018.6532.

[18] K. Liu, X. Li, Y. Gao, Y. Cheng, H. Wang, and Y. Qin, "High-resolution electromagnetic vortex imaging based on sparse Bayesian learning," *IEEE Sensors J.*, vol. 17, no. 21, pp. 6918–6927, 1, Nov. 2017, doi: 10.1109/JSEN.2017.2754554.

[19] M. J. Jahromi and M. H. Kahaei, "Two-dimensional iterative adaptive approach for sparse matrix solution," *Electron. Lett.*, vol. 50, no. 1, pp. 45–46, Jan. 2014, doi: 10.1049/EL.2013.2159.
[20] T. Yuan, Y. Cheng, H.-Q. Wang, and Y. Qin, "Generation of OAM radio beams with modified uniform circular array antenna," *Electron. Lett.*, vol. 52, no. 11, pp. 896–897, May 2016, doi: 10.1049/EL.2016.0269.

CONG ZHANG was born in Xinyang, China, in 1996. He received the bachelor's degree from Tsinghua University, Beijing, China, in 2017. He is currently pursuing the Ph.D. degree with Air Force Engineering University. His major is information and communication engineering. His research interests include vortex electromagnetic wave radar imaging processing and complex target recognition.

HANG YUAN was born in Guangdong, China, in 1997. He received the bachelor's degree from the South China University of Technology (SCUT), China, in 2019. He is currently pursuing the master's degree with Air Force Engineering University. His major is information and communication engineering. His main research interests include radar imaging processing and target recognition.

QUN ZHANG received the M.S. degree in mathematics from Shaanxi Normal University, Xi'an, China, in 1988, and the Ph.D. degree in electrical engineering from Xidian University, Xi'an, in 2001.

He was a Research Engineer and a Research Fellow with the Department of Electrical and Computer Engineering, National University of Singapore, Singapore, from 2001 to 2003 and from 2005 to 2006, respectively. He is currently a Professor with the Institute of Information and Navigation, Air Force Engineering University, Xi'an, and an Adjunct Professor with the Key Laboratory for Information Science of Electromagnetic Waves, Ministry of Education, Fudan University, Shanghai, China. He has published over 200 papers on journals and conferences. His main research interests include signal processing, clutter suppression, and its application in SAR and ISAR.

YING LUO was born in Hunan, China, in 1984. He received the M.S. degree in electrical engineering from the Institute of Telecommunication Engineering, Air Force Engineering University (AFEU), Xi'an, China, in 2008, and the Ph.D. degree in electrical engineering from AFEU, in 2013.

He was a Postdoctoral Fellow with the National Laboratory of Radar Signal Processing, Xidian University, from 2014 to 2017, and a Visiting Scholar with the Department of Electrical and Computer Engineering, National University of Singapore, Singapore, from 2017 to 2018. He is currently a Professor/a Ph.D. Advisor with the Institute of Information and Navigation, AFEU. He is also an Adjunct Associate Professor with the Key Laboratory for Information Science of Electromagnetic Waves, Ministry of Education, Fudan University. He has published three books and over 100 papers on journals and conferences. Two of these papers won the First-Grade Prize of Shaanxi Natural Science Excellent Academic Paper, in 2010 and 2013, respectively. His research interests include signal processing and auto target recognition (ATR) in SAR and ISAR.